Supporting Information

Complex molecular dynamics of symmetric model discotic liquid crystals: Comparison of Hexakis(hepta-alkanoyloxy)triphenylene (HOT6) with Hexakis(hexa-alkyloxy)triphenylene (HAT6).

Christina Krause[1], Paulina Szymoniak[1], Wiebke Lohstroh[2], Fanni Juranyi[3], Michaela Zamponi[4], Bernhard Frick[5], Dominik Al-Sabbagh[1], Franziska Emmerling[1,6], Reiner Zorn[7], Andreas Schönhals[1,8,*]

[1]Bundesanstalt für Materialforschung und -prüfung (BAM), Unter den Eichen 87, 12205 Berlin, Germany

[2]Heinz Maier-Leibnitz Zentrum (MLZ), Technische Universität München, Lichtenbergstraße 1, 85748 Garching, Germany

[3]PSI Center for Neutron and Muon Sciences, 5232 Villigen PSI, Switzerland

[4]Forschungszentrum Jülich GmbH, Jülich Centre for Neutron Science at MLZ, Lichtenbergstr. 1, 85748 Garching, Germany

[5]Institut Laue-Langevin, 71 avenue des Martyrs, 38042 Grenoble Cedex 9, France

[6]Institut für Chemie, Humboldt Universität zu Berlin, Brook-Taylor-Straße 2, 12489 Berlin Germany

[7]Forschungszentrum Jülich GmbH, Jülich Centre for Neutron Science (JCNS-1), 52425 Jülich, Germany

[8]Institut für Chemie, Technische Universität Berlin, Straße des 17. Juni 135, 10623 Berlin, Germany

[*]CORRESPONDING AUTHOR: A. Schönhals, BAM Bundesanstalt für Materialforschung und -prüfung (Department Materials Chemistry), Unter den Eichen 87, 12205 Berlin, Germany; Tel. +49 30 / 8104-3384; Fax: +49 30 / 8104-73384; Email: Andreas.Schoenhals@bam.de

Calculation of the scattering cross-sections:

Calculation of the neutron cross sections for the materials used. The total cross sections were obtained by multiplication of the individual nuclear cross sections with the number of respective nuclei in the monomeric units. This procedure is correct for incoherent scattering and absorption; for coherent scattering it represents the high-q limit. The absorption cross sections were corrected to the actual wavelength of the experiments, and therefore the tabulated values are multiplied a factor 4.64 Å / 1.8 Å in addition.

HOT6

Number	Atom	coh. ind.	coh. total	inc. ind.	inc. total	abs. ind.	abs. total
60	C	5.551	333.06	0.001	0.06	0.0035	0.653
84	H	1.7568	147.571	80.26	6741.84	0.3326	86.919
12	O	4.232	50.784	0.0008	0.0096	0.00019	0.007
Total / Molecule:			531.4152		6741.91		87.579

The unit of the data are 10^{-24} cm^2

Raw data neutron scattering:

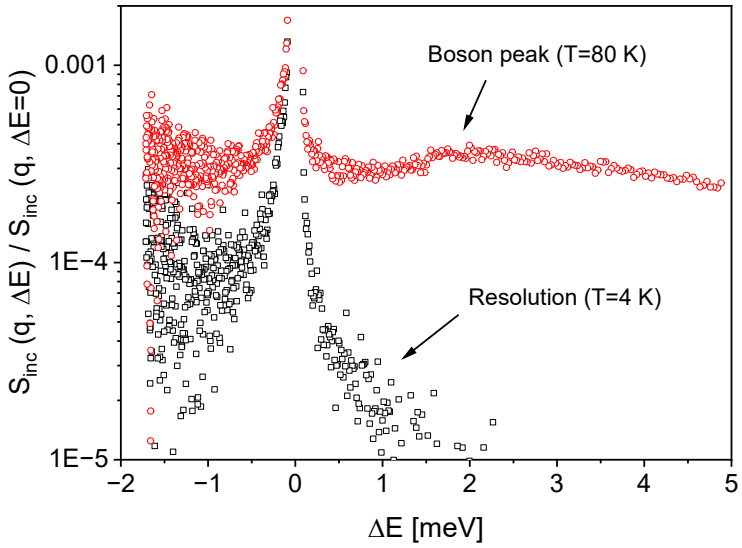

Figure S1: Inelastic TOFTOF spectra for HOT6 at a scattering angle of 98.6 ° (elastic q=1.7 $Å^{-1}$) normalized to the height of the elastic line: Black squares – resolution of TOFTOF measured at 4 K. Red circles – Inelastic scattering measured at 80 K. ΔE is the measured energy transfer.

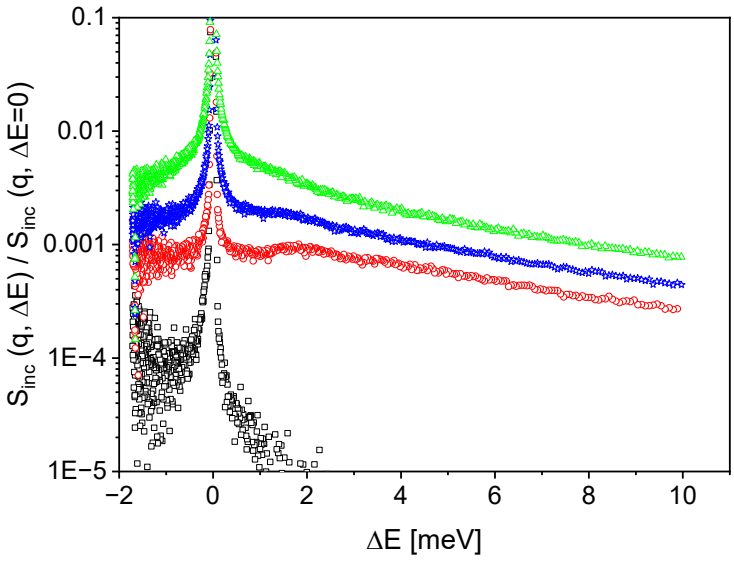

Figure S2: Quasielastic TOFTOF spectra for HOT6 at a scattering angle of 98.6 ° (elastic q=1.7 $Å^{-1}$) normalized to the height of the elastic line: Black squares – resolution of TOFTOF measured at 4 K. Red circles – T=150 K. blue asterisks - T=200 K and green triangles - T=250 K. ΔE is the measured energy transfer.

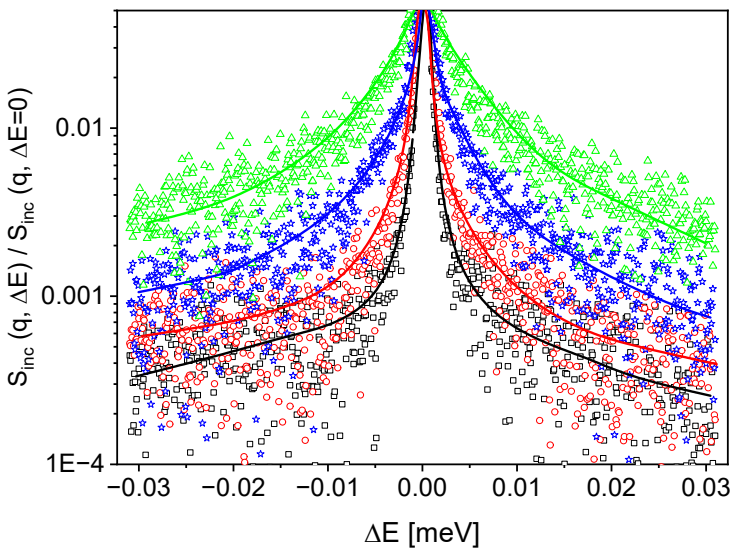

Figure S3: Quasielastic SPHERES spectra for HOT6 at a scattering angle of 90 ° (q=1.42 $Å^{-1}$) normalized to the height of the elastic line: Black squares – resolution of SPHERES measured at 4 K. Red circles – T=150 K. blue asterisks - T=200 K and green triangles - T=250 K. ΔE is the measured energy transfer. The lines are guides to the eyes. Only data points are used for further analysis.

Section fitting of dielectric data by the HN-function:

Direct fit of the HN-function:

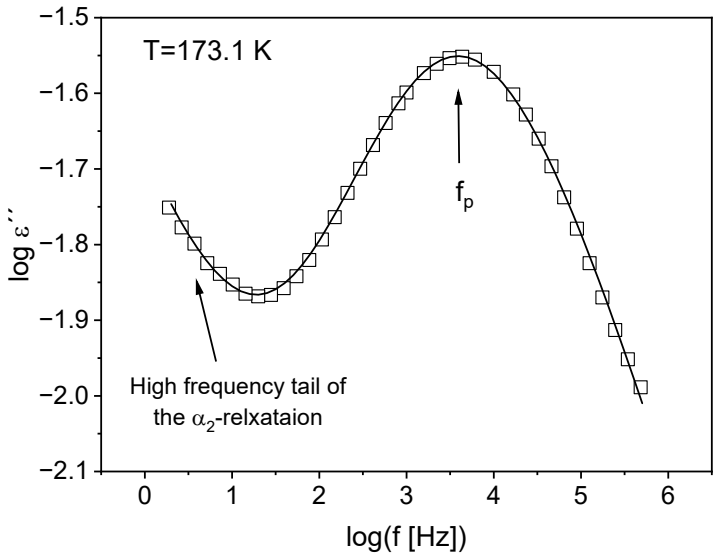

Figure S4: Example for a fit of a single HN-function to the data of HOT6 at T=173.1 K. The line is the fit of the HN-function to the data including a power law for the contribution of the high frequency tail of the α_2-relaxation which is located at lower frequencies.

To analyze the dielectric γ-relaxation and parts of the α_2-process, the Havriliak-Negami (HN) model function is fitted to the experimental data. The HN function is mathematically given by[1]

$$\varepsilon^*_{HN}(\omega) = \varepsilon_\infty + \frac{\Delta\varepsilon_{HN}}{(1 + (i\omega\tau_{HN})^{\beta})^{\gamma}}. \quad \text{(S1a)}$$

ε_∞ denotes the real part of the complex function in the limit $\varepsilon_\infty = \lim_{\omega \gg \tau_{HN}^{-1}} \varepsilon'(\omega)$. $\Delta\varepsilon_{HN}$ signifies the dielectric strength. The relaxation time, τ_{HN}, is associated with the frequency at which the dielectric loss has its peak maximum value, referred to as f_p (relaxation rate). f_p is calculated from the relaxation time using the following relationship[2]

$$f_p = \frac{1}{2\pi\,\tau_{HN}}\left[sin\frac{\beta\pi}{2+2\gamma}\right]^{1/\beta}\left[sin\frac{\beta\gamma\pi}{2+2\gamma}\right]^{-1/\beta}. \quad \text{(S2)}$$

The parameters β and γ ($0 < \beta$; $\beta\gamma \leq 1$) are used to describe the symmetric and asymmetric broadening of the relaxation spectrum relative to the Debye model.[2] If conductivity related effects overlay the relaxation process they are accounted for by incorporating the term

$\frac{\sigma_0}{(\omega^s \varepsilon_0)}$ into the dielectric loss part of the HN-function. The parameter σ_0 is related to the DC conductivity but also encompasses contributions from Maxwell-Wagner-Sillars effects and/or electrode polarization. The parameter $0<1s\leq 1$ characterizes non-ohmic effects in conductivity, with s=1 indicating ohmic conductivity. The symbol ε_0 represents the permittivity of free space. An example for the fit of the HN-function to the γ-relaxation of HOT6 is given in Figure S4 including a power law to model the high frequency tail of a relaxation process which is located at lower frequencies.

In the case that several relaxation processes were observed in the accessible frequency window a sum of HN-functions were fitted to the data of the dielectric data. In that case the complete fit function reads

$$\varepsilon^*{}_{fit}(\omega) = \varepsilon_\infty + \sum_k \frac{\Delta\varepsilon_{HN,k}}{\left(1 + \left(i\omega\tau_{HN,}\right)^{\beta_k}\right)^{\gamma_k}} - i\frac{\sigma_0}{\left(\omega^s \varepsilon_0\right)} \qquad \text{(S1b)}$$

k counts the different processes observed in the available frequency window. For further details, refer to ref. 2.

Derivative approach (Conduction free loss):

In cases where the dielectric loss is dominated by conductivity, or the relaxation processes strongly overlap the dielectric spectra can be analyzed by a so-called conduction free loss approach.[3] For the Debye function it could be shown that

$$\varepsilon''_{Deriv} = -\frac{\pi}{2}\frac{d\,\varepsilon'}{d\ln(\omega)} = \varepsilon''^2 \qquad \text{(S3)}$$

holds. By this approach the contributions of the Ohmic conductivity are removed. Moreover, due to the square in ε''_{Deriv} the width of the conduction free loss is smaller than that of ε′′ itself. The power of this technique is demonstrated by Figure S5 where the frequency dependence of ε′′ is compared to that of ε''_{Deriv}.

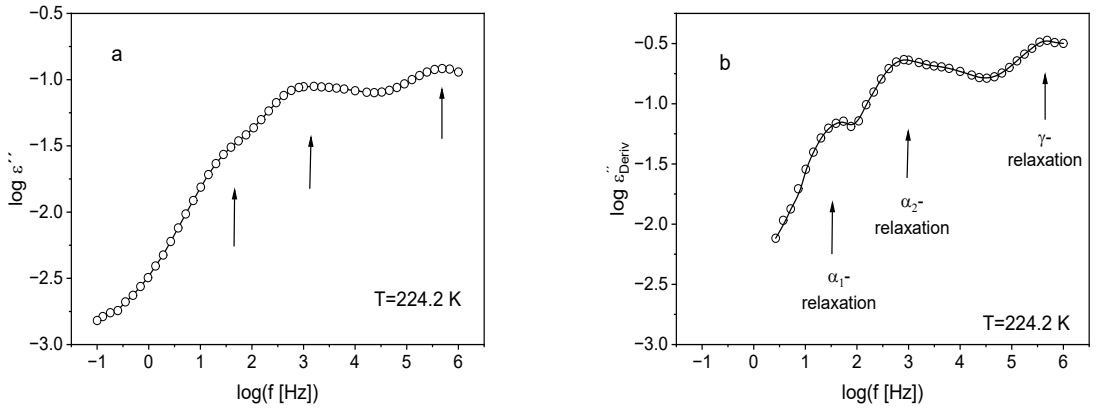

Figure S5: a – Dielectric loss versus frequency for HOT6 at a temperature of 224.2 K. The line is a guide for the eyes. b - ε''_{Deriv} versus frequency for the same data depicted in part a of the figure. The line is a fit of eq. S4c involving three relaxation processes.

Figure S5a depicts the dielectric loss versus frequency for HOT6 at a temperature of 224.2 K. The spectra show three broad strongly overlapping relaxation processes which are hard to analyze reliably without additional assumptions. For comparison Figure S5b gives the conduction free loss ε''_{Deriv} for the same data given in Figure S5a. Three well separated relaxation processes are observed characterized as distinctive peaks in ε''_{Deriv}.

The frequency dependence of ε''_{Deriv} is analyzed by fitting the derivative of the real part of the HN-function $\frac{d\,\varepsilon'_{HN}}{d\ln\omega}$ to the data. $\frac{d\,\varepsilon'_{HN}}{d\ln\omega}$ is given by

$$\varepsilon''_{Deriv,HN} = \frac{d\epsilon'_{HN}}{dln\omega} = -\frac{\beta\gamma\Delta\epsilon_{HN}(\omega\tau_{HN})^{\beta}\cos\left(\frac{\beta\pi}{2}\right)(-(1+\gamma)\Psi(\omega))}{\left[1+2(\omega\tau_{HN})^{\beta}\cos\left(\frac{\beta\pi}{2}\right)+(\omega\tau_{HN})^{2\beta}\right]^{\frac{1+\gamma}{2}}} \quad \text{(S4a)}$$

with

$$\Psi(\omega) = \arctan\left[\frac{\sin\left(\frac{\beta\pi}{2}\right)}{(\omega\tau_{HN})^{-\beta}+\cos\left(\frac{\beta\pi}{2}\right)}\right]. \quad \text{(S4b)}$$

In the case that several relaxation processes were observed in the accessible frequency window a sum of $\varepsilon''_{Deriv,HN}$ contributions is fitted to the experimental data of ε''_{Deriv}. The whole fit function then reads

$$\epsilon''_{Deriv,fit}(\omega) = \sum_k \varepsilon''_{Deriv,HN,k}(\omega) + \frac{C}{\omega^{\delta}} . \quad \text{(S4c)}$$

k counts the number of the different relaxation processes. The term models $\frac{C}{\omega^{\delta}}$ possible polarization effects which are not resolved by the derivative approach. An example of fitting the derivative involving three relaxation processes is given in Figure S5b.

Section Fast scanning calorimetry

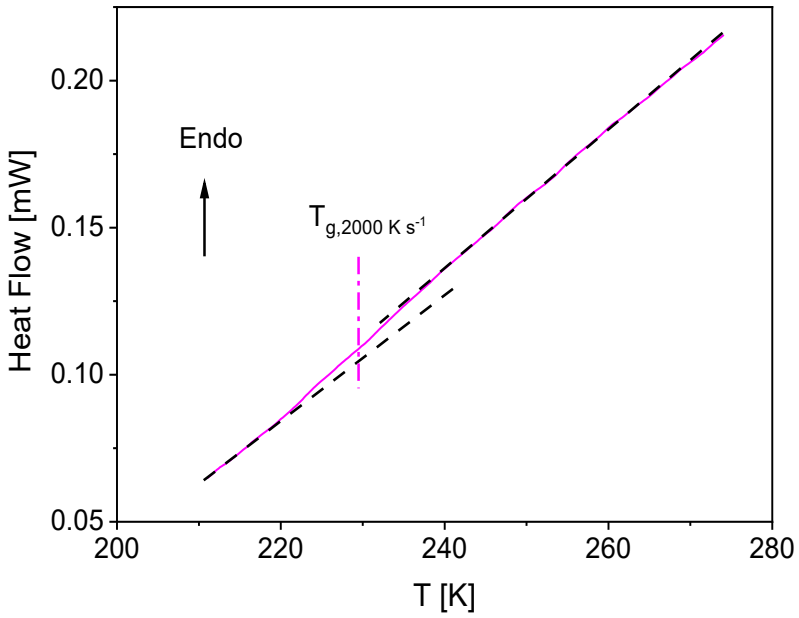

Figure S6: Heat flow versus temperature for HOT6 measured with fast scanning calorimetry with a heating rate of 2000 K s^{-1}.

Comparison of different calculation methods for the effective mean squared displacements

Figure S6 compares the temperature dependence of the effective mean squared displacement $\langle u^2 \rangle_{eff}$ for HAT6 calculated by eq. 4 and be the method given in ref. 4. In general, $\langle u^2 \rangle_{eff}$ calculated by both methods is similar. However, the values calculated by eq. 4 are higher than that calculated by the method given in ref. 4. This demonstrates that the value of an *effective* mean squared displacement depends strongly on its definition. This is a consequence of the true $\langle u^2 \rangle$ being a function of time unless $S_{inc}(q,t)$ shows a clear plateau. While in the algorithm of ref. 4 it is attempted to reconstruct the value of $\langle u^2 \rangle$ at a certain time using a fractal model, here we use an approach which is closer to the common $\ln I_{el}(q)$ vs. q plot. This procedure includes a time scale only implicitly via the width of the resolution function of the instrument used. But because the same procedure was used for HAT6 and HOT6 and IN16B and IN16 have identical resolution, this is sufficient for a qualitative comparison.

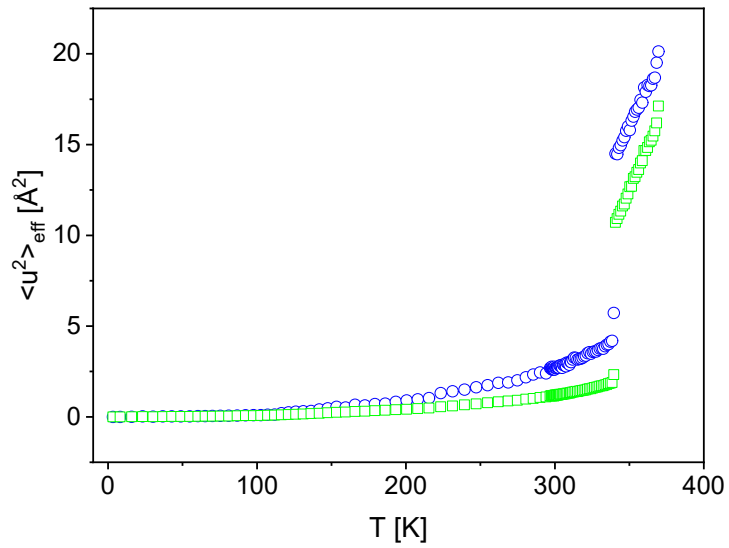

Figure S7: Comparison of the effective mean squared displacement $\langle u^2 \rangle_{eff}$. Blue circles – calculated by eq. 4, green squares – calculated according to the method given in ref. 4.

Calculation of the VDOS

More details about are available in the supporting information of ref. 5. In the first step, the VDOS is calculated from the one-phonon expression of the incoherent scattering function by eq. 9b yielding $\tilde{g}(q,\omega)$ for each detector group. The result should be the same for all detector groups because $g(\omega)$ is a material property. Instead, it shows a q dependence which is mostly due to multiple scattering. With some reasonable assumptions, multiple scattering results in a $1/q^2$ term:

$$\tilde{g}(q,\omega) = g(\omega)\left(1 + f_{MS}/q^2\right) \tag{S6}$$

The parameter f_{MS}, defining the strength of multiple scattering, is determined by a fit of the integral of $g(\omega)/\omega^2$ over a region providing good statistics, here: $2.0\cdots4.6\ ps^{-1}$ for HAT6/IN6 and $2.1\cdots5.0\ ps^{-1}$ for HOT6/TOFTOF. Figure S8 shows the integral plotted versus the elastic $1/q^2$. The result is obtained by correcting all preliminary values $\tilde{g}(q,\omega)$ by $1/\left(1 + f_{\mathrm{MS}}/q^2\right)$ and subsequent averaging.

$$\int_{2.0|2.1\ \mathrm{ps}^{-1}}^{4.6|5.0\ \mathrm{ps}^{-1}} \frac{g_{calc}(q,\omega)}{\omega^2}\,\mathrm{d}\omega$$

Figure S8: Plot of the integral vs elastic q^{-2} and fit with eq. S6. HAT6/IN6 (blue): uncorrected VDOS values (squares), fit (continuous line). HOT6/TOFTOF (red): uncorrected VDOS values (crosses), fit (dashed line).

References

[1] Havriliak, S.; Negami, S. A Complex Plane Analysis of α-Dispersions in Some Polymer Systems. *Journal of Polymer Science Part C: Polymer Symposia* **1966**, *14*, 99–117.
[2] Schönhals, A.; Kremer, F. Analysis of Dielectric Spectra. In *Broadband Dielectric Spectroscopy*; Kremer, F., Schönhals, A., Eds.; Springer: Berlin, Heidelberg, **2003**; pp 59–98.
[3] Wübbenhorst, M.; van Turnhout, J. Analysis of Complex Dielectric Spectra. I. One-Dimensional Derivative Techniques and Three-Dimensional Modelling. *Journal of Non-Crystalline Solids* **2002**, 305, 40–49.
[4] Zorn, R. On the evaluation of neutron scattering elastic scan data. *Nucl. Instr. Meth. A* 2009, **603**, 439-445.
[5] Schönhals, A.; Zorn, R.; Kruteva, M.; Ahmadi, S.; Juranyi, F.; Szymoniak, P. Local mechanical invariance in a recycled bio-based vitrimer: Evidence from the vibrational density of states. *Macromolecules* **2025**, submitted